Chemistry Europe
European Chemical Societies Publishing

WILEY VCH

Excellence in Chemistry Research

Announcing our new flagship journal

- Gold Open Access
- Publishing charges waived
- Preprints welcome
- Edited by active scientists

Meet the Editors of *ChemistryEurope*

Luisa De Cola
Università degli Studi di Milano Statale, Italy

Ive Hermans
University of Wisconsin-Madison, USA

Ken Tanaka
Tokyo Institute of Technology, Japan

ChemistrySelect

Research Article
doi.org/10.1002/slct.202200697

Chemistry Europe
European Chemical Societies Publishing

www.chemistryselect.org

Production and Characterization of PLA/HA/GO Nanocomposite Scaffold

Busra Oktay,[a] Esma Ahlatcıoğlu Özerol,[a] Ali Sahin,[b] Oguzhan Gunduz,[c, d] and Cem Bulent Ustundag*[a]

Polylactic acid (PLA) composite nanofibers combined with hydroxyapatite (HA) and graphene oxide (GO) nanoparticles were produced by electrospinning to create excellent biodegradable and durable scaffolds to be used in tissue engineering. The properties of the pure PLA, PLA/HA, PLA/GO, and PLA/HA/GO nanocomposite scaffolds were analyzed in chemical, morphological, mechanical, and biocompatibility. Morphology and composition were investigated by scanning electron microscopy (SEM) and Fourier transform infrared spectroscopy (FTIR), respectively. To predict the cytocompatibility of these scaffolds, HFF-1 cells were cultured and the respective cell adhesion and proliferation were investigated by fluorescence microscopy, SEM, and MTT assay. FTIR results showed the successful synthesis of HA and GO nanoparticles. SEM images showed that the PLA/HA/GO scaffold is ideal for cell attachment and proliferation in tissue regeneration. Mechanical test results showed that the tensile strength and elastic modulus of PLA nanofibers could be increased by adding 0,8 wt % HA and 0,4 wt % GO. The PLA/HA/GO scaffold exhibited the highest tensile strength of other scaffolds. MTT assay revealed that the PLA/HA/GO scaffold showed significantly high biocompatibility with 105 % cell viability. Therefore, PLA/HA/GO scaffold with 0,8 wt %HA and 0,4 wt %GO possessing high tensile strength as well as good cell proliferation is an excellent and versatile biomaterial for tissue engineering applications.

Introduction

Tissue engineering is a multidisciplinary field that combines biology, medicine, and engineering methods. It works for the regeneration of tissues that have lost their function as a result of damage to tissues and organs, or for the formation of new tissue.[1] Today, there are tissue engineering applications for the regeneration of damaged tissue in a short time without immunological problems.[2] The tissue engineering method includes tissue support that maintains and supports cell attachment and functionality, a rich source of cells selected according to the target tissue, and growth factors or cellular signals that control the behavior of these cells.[4–6] One of the tissue engineering applications is to create functional tissue by designing a scaffold.[3] Scaffolds are mainly applied to create a physically and mechanically stable tissue-like structure. Tissue formation occurs thanks to biomolecules that direct the organization, growth, and differentiation of cells placed on the scaffold.[8,9] Scaffolds not only form a suitable adhesion surface for cells but also help to interact with the environment-tissue to respond to physiological and biological changes.[10] It must be highly porous to allow cellular migration and passage of nutrients into cells within the structure.[11] The selection of the material to be used in the production of scaffold is important. Biomaterials interact with the body, affect biological processes, and promote tissue regeneration. Scaffolds need to be made of biocompatible and biodegradable materials and support cell adhesion, differentiation, and growth.[12–14] Polymers used as biomaterials can be preferred as natural or synthetic. Although natural polymers are more biocompatible than synthetic polymers, synthetic polymers offer more possibilities for chemical modifications and molecular changes that can be adapted to facilitate scaffold adaptation.[15] Synthetic polymers can be produced with a special structure and the degradation rate of these polymers can be controlled quite easily.[16] Synthetic polymers can be formed as scaffolds by adapting properties such as pore size, porosity, degradation rate, and mechanical strength.[17] Bioceramics are used in tissue engineering applications as biomaterials. The distinctive features of bioceramic scaffolds are very low elasticity and high mechanical stiffness. Thanks to these features, they have a hard and brittle surface. From the bone point of view, they exhibit excellent biocompatibility due to their chemical and structural similarity to the mineral phase of native bone.[18] Carbon-based nanoparticles are used as biomaterials in scaffolds, thanks to their outstanding mechanical properties and large surface areas that facilitate interactions with biomolecules.[19] There are

[a] *B. Oktay, Assoc. Prof. Dr. E. Ahlatcıoğlu Özerol, Assoc. Prof. Dr. Cem Bulent Ustundag*
Department of Bioengineering,
Faculty of Chemical and Metallurgical Engineering,
Yildiz Technical University,
Istanbul, 34220, Turkey
E-mail: cbustun@yildiz.edu.tr
cbustundag@gmail.com
[b] *Ali Sahin*
Department of Biochemistry, Faculty of Medicine,
Marmara University,
Istanbul, 34854, Turkey
[c] *Assoc.Prof. Dr. Oguzhan Gunduz*
Center for Nanotechnology & Biomaterials Application and Research (NBUAM), Marmara University,
Istanbul, 34730, Turkey
[d] *Assoc.Prof. Dr. Oguzhan Gunduz*
Department of Metallurgical and Materials Engineering,
Faculty of Technology, Marmara University,
Istanbul, 34730, Turkey

disadvantages as well as advantages to scaffolds produced from a single biomaterial. Composite scaffolds, a combination of ceramic and polymer or synthetic polymers with natural polymers, are the best solution to overcome these disadvantages.[20] The mechanical properties, cell behavior, and degradation rate of the scaffold are improved by combining an inorganic material which has good toughness and compressive strength and a polymer with high bioactivity.[21] Nanostructured scaffolds outperform for tissue engineering applications according to microstructured scaffolds. The electrospinning technique is also used in tissue engineering applications to produce nanostructured scaffolds by producing biocompatible nanofibers.[22] The electrospinning method is one of the simplest of all methods used to prepare extracellular matrix-like fibers. Electrospinning allows the pore size of the fibers to be reduced from micrometer to nanometer diameter, thereby increasing the surface area/volume or mass ratio.[23] The advantages of the electrospinning technique are easy functionality for a variety of applications, superior mechanical properties and large surface area on the scaffold, and the production of very fine fibers.[24] Electrospun scaffolds allow cells to adhere, grow and differentiate while providing adequate mechanical support according to the structure and properties of the biopolymer.[25] The scaffold in a biopolymeric structure should be biocompatible, biodegradable, and allow tissue exchange.[26] PLA is created by the polymerization of lactic acid and is derived from renewable resources, including starch and sugar.[27] It has been used to make a number of medical implants, including bone screws, fixation devices, and vascular grafts.[28] Several different forms of PLA exist due to the chiral nature of lactic acid, including poly-L-lactide (PLLA) and poly-D-lactide (PDLA), which are produced from the polymerization of L-lactide and D-lactide, respectively.[36] PLA is used to construct a scaffold for tissue engineering thanks to its good biodegradability and biocompatibility.[29] The interaction of osteogenic cells with ceramics is important for bone regeneration, as ceramics can increase osteoblast differentiation and proliferation.[9] Hydroxyapatite ($Ca_{10}(PO_4)_6(OH)_2$) has a chemical composition similar to the inorganic component of natural bone and exhibits extraordinary biocompatibility, bioactivity, and osteoconductivity properties, so it is one of the main materials used in bone tissue engineering.[30] It also provides the material with non-toxic and non-inflammatory properties.[24] The mechanical properties of HA vary from the size of the particles, porosity, density, etc.[31,32] are affected by situations. HA is very hard but brittle, has a very slow rate of degradation in vivo, and is combined with natural or synthetic polymers to form scaffolds whose degradation rate can be controlled. On the other hand, HA is very beneficial in bone formation as it stimulates growth factors (for example, bone morphogenic protein) and promotes alkaline phosphatase (ALP) in mesenchymal stem cells.[33] The compositional similarity of HA with bone, and its osteoinductive and osteoconductive properties allow HA-containing structures to form a strong bond with the bone.[34] Due to its chemical similarity to natural bone, HA is combined with PLA polymer to provide biocompatibility and biodegradability properties to the scaffold and facilitate osteoconductivity properties and good differentiation and proliferation of cells.[30] Graphene oxide (GO) is obtained by the oxidation of graphene. GO has oxygen-containing functional groups that can bind to biomolecules. These functional groups are epoxy, hydroxyl, carboxyl, and carbonyl. These functional groups show better mechanical, biocompatibility, and bioactivity properties in bioapplications.[35,36] GO contains both hydrophobic and hydrophilic regions due to its amphiphilic property. The hydrophilic region allows the functionalization of graphene oxide. Hydroxyl and carboxyl functional groups give GO better hydrophilicity than graphene.[36] These groups allow GO to form a strong interfacial bond between the filler and the matrix. The hydrophobic region, on the other hand, attracts drugs, genes, or other molecules through electrostatic attraction. Thus, since the interaction properties of the material are increased, it is easily used in bioapplications.[37,38] GO was added to the polymeric structure to increase the mechanical strength of the scaffold and the surface area to interact with biomolecules.[39,40] These composite-based nanofibers were produced by the electrospinning method.

Polylactic acid (PLA) is a polymer used in many fields due to its biodegradability and biocompatibility, but its disadvantages such as mechanical weakness and water solubility ratio have been limited.[36] In order to overcome these limitations and improve the properties of PLA nanofibers produced by electrospinning, it is recommended that PLA polymer composite with suitable materials. Therefore, it is aimed to increase the mechanical and biocompatibility properties of polymeric-based composite nanofiber structure scaffolds by adding HA and GO to PLA for use in tissue engineering. This study aimed to produce a biocompatible scaffold with sufficient mechanical properties by electrospinning method to be used in tissue engineering applications. Accordingly, this study includes new approaches and values in tissue engineering to produce PLA nanocomposite scaffolds that are more durable and will increase the adhesion of cells.

Results and Discussion

A piece of each fabricated nanocomposite scaffold by the electrospinning method is shown in Figure 1. They were very thin, fibrous, and elastic. The fibrous structure requires that they could be very porous. They have nano-sized pores thanks to electrospinning.

Crystal Structure Analysis of Nanoparticles

Structural analysis of HA was done by X-ray powder diffraction. The XRD models of HA are shown in Figure 2. The XRD pattern of HA contains sharp peaks indicating good crystallinity. The characteristic peaks of HA in the XRD model are approximately $2\theta = 31{,}60°$. In addition, as seen in Figure 2(a), the peaks belonging to the 002, 211, 300, 130, 222 planes are also seen in the XRD model. Accordingly, it is seen that HA was synthesized correctly. Meanwhile, when we compare the results with the literature, the diffraction peaks indicated that the obtained HA particles have excellent osseointegration properties.[44]

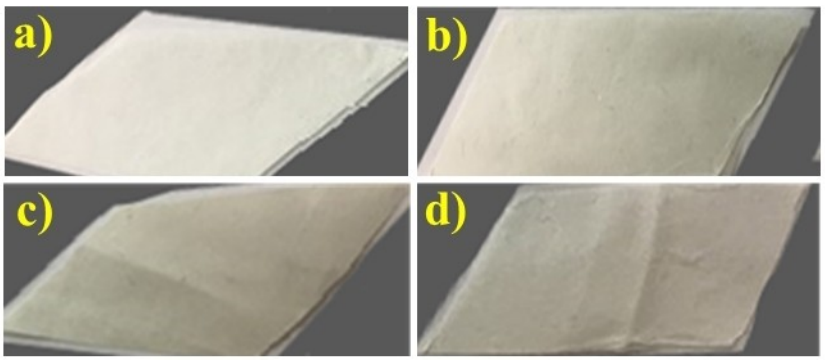

Figure 1. A piece of fabricated nanofibers. PLA (a), PLA/HA(b), PLA/GO(c), PLA/HA/GO(d).

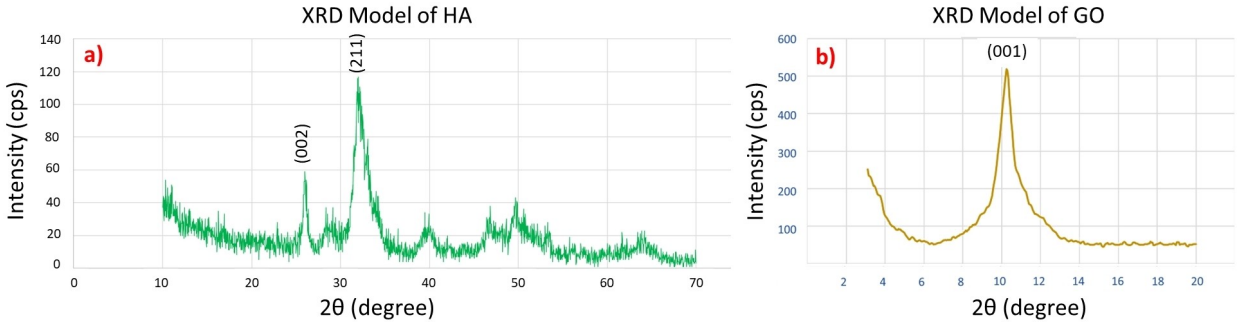

Figure 2. XRD model of HA(a) and GO(b).

The XRD model of synthesized GO is used to examine the change between layers of the material and its crystal properties. When the characteristic peaks in the XRD model are compared with the results in the literature, it is seen that $2\theta = 26.4636°$ for graphite and $2\theta = 10.524°$ for GO. In Figure 2(b), after oxidation the absence of the graphite peak in GO instead the 10.5524° peak presence that is about GO is in agreement with the results in the literature and shows that GO has been synthesized successfully.[45]

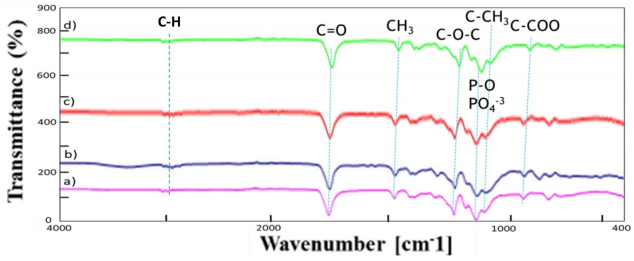

Figure 3. FT-IR spectra of PLA, PLA/HA, PLA/GO, PLA/HA/GO nanofibers. PLA nanofibers (a), PLA/HA nanofibers (b), PLA/GO nanofibers (c), PLA/HA/GO nanofibers (d).

Chemical Structure Analysis

FTIR analysis was carried out to investigate the functional groups of nanofibers of PLA, PLA/HA, PLA/GO and PLA/HA/GO. As can be seen from the FTIR spectra (Figure 3), all scaffolds showed similar absorption peaks to the characteristic spectrum of pure PLA. All nanofibers were determined to be very similar to that pure PLA nanofibers due to the overlapping of HA and GO vibrational bands ranging from 1800 to 1000 cm^{-1}. The spectrum of PLA shows a sharp absorption band at 1737 cm^{-1} attributed to the stretching vibration of the carbonyl group (C=O) in the PLA. No clear characteristic peaks for GO or HA were observed on the FTIR spectra of the nanocomposites, probably because PLA was more sensitive to infrared rays than that GO, and the characteristic peaks of the scaffold were covered by PLA.[46] It appears that some peaks of GO and HA are absent in the spectrum of the scaffold, this indicates that the particles probably are well dispersed in the scaffold matrix. It is thought that the similarity of PLA/HA/GO nanofibers to pure PLA nanofibers, is that the nanoparticles are well dispersed in the polymer matrix and that the nanoparticles bond strongly with PLA.[47] On the other hand, PLA was used more intensely than GO and HA. Because of this reason, at the FTIR Spectra was used much less than PLA for this study. HA and GO spectra may not have been visualized because PLA was used intensely.

Morphological Observation of the Nanofibers

To obtain ideal nanofibers, it is important to mix the nanoparticles in the solution and disperse them in the solution. SEM

images of PLA and PLA/HA/GO are shown in Figure 4. It can be observed that all the fibers were in nanoscale and randomly distributed. The diameter of the nanofiber and the solution concentration used in electrospinning are directly proportional to each other. As the concentration increases, the nanofiber diameter also increases. Besides, when electrical conductivity increases, nanofibers usually result in smaller.[43,48] So, looking at the results with the same magnification, it is seen that diameter of PLA/HA/GO fibers has finer fibers than the diameter of PLA fibers. This was due to the solution concentration of PLA decreasing by adding a solution containing GO and HA to PLA. And also, the significant increase in conductivity for PLA/GO was caused by the negatively charged GO from the hydroxyl, carboxyl, and epoxy groups on its surface that were produced during the oxidation process.[46] Therefore, PLA/HA/GO nanofibers may be thinner. According to the SEM images, pure PLA nanofibers (Figure 4(a)(b)) showed a relatively smooth surface structure and PLA/HA/GO composite nanofibers (Figure 4(c)(d)) showed a highly rough surface structure. It was observed that the roughness of nanofibers increased when HA/GO nanoparticles were added to PLA. Thanks to the increased surface roughness in nanofibers with the addition of GO and HA nanoparticles, it was predicted that PLA/HA/GO nanofibers form a potential scaffold to promote cell adhesion and growth.[49]

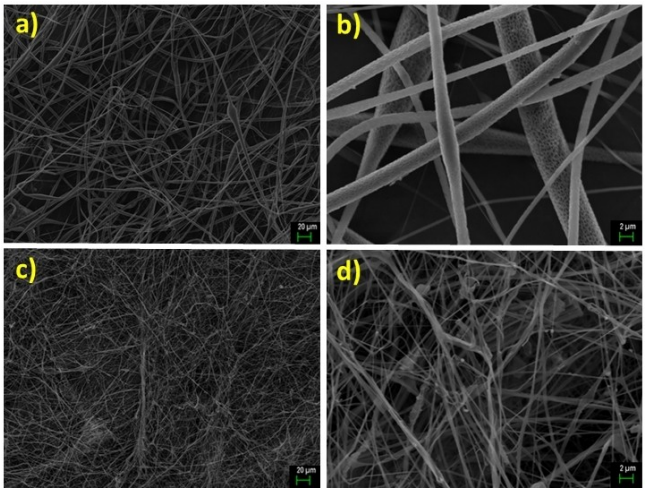

Figure 4. SEM images of fabricated nanofibers. The low resolution of pure PLA(a) and PLA/HA/GO(c), the high resolution of pure PLA(b) and PLA/HA/GO(d).

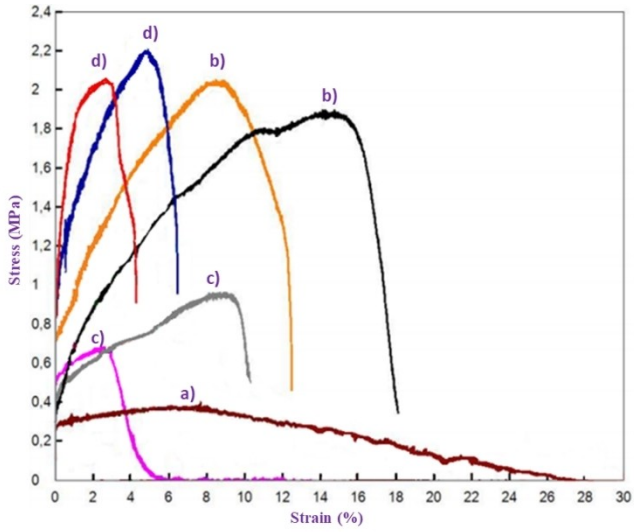

Figure 5. Stress-strain plot of nanofibers as a result of mechanical testing. PLA (a), PLA/GO (b), PLA/HA (c), PLA/HA/GO (d).

Mechanical Testing

Mechanical tests are important in determining the stability and integrity of the scaffold. To determine the strength and flexibility of the produced nanofibers, tensile tests were performed on PLA, PLA/HA, PLA/GO, PLA/HA/GO nanofibers. The stress-strain curves of nanofibers at break are shown in Figure 5. The average of the tensile strength (MPa) and breaking stress (%) values of nanofibers produced by the electrospinning method are given in Table 1.

According to Table 1, elongation of pure PLA nanofiber is ~25%, and elongation of PLA/HA/GO nanofiber is ~6%. In Figure 5, it was seen that the elasticity of the PLA/HA/GO composite structure decreased and the modulus of elasticity (tensile (MPa)/strain (%)) increased compared to the pure PLA nanofiber. The modulus of elasticity; is a value that indicates the rigidity of the material. The greater the modulus of elasticity, the more rigid the material and the smaller the elastic strain.[50] As a result of the strong matrix interaction of GO nanolayers with PLA, an increase in the strength of PLA/GO fibers was observed. According to Table 1, it was obtained that PLA/GO nanofibers showed better mechanical strength and elongation properties than PLA/HA nanofibers. This is because HA is bioceramic and brittle.

Mechanical test results showed that the tensile strength and elastic modulus of PLA nanofibers could be increased by adding 0,8 wt% HA and 0,4 wt% GO. The PLA/HA/GO composite scaffold exhibited higher tensile strength than the other scaffolds. PLA/HA/GO showed the most resistance to stress, and the best durability.[20] Based on these results, it can be said that the produced PLA/HA/GO nanofibers are good candidates for tissue engineering applications.

Cell viability/Cytotoxicity Test (MTT)

Fibroblast cells (HFF-1) were used to examine the cytocompatibility of the nanofiber scaffolds. The viability of cells on the

Table 1. Mechanical properties of PLA, PLA/HA, PLA/GO, and PLA/HA/GO scaffolds.

Scaffold	Tensile Strength (MPa)	Elongation (%)
PLA	0.38 ± 0.1	27.08 ± 2.02
PLA/HA	0.84 ± 0.13	12.1 ± 1.5
PLA/GO	1.97 ± 0.14	15.28 ± 2.81
PLA/HA/GO	2.18 ± 0.09	5.37 ± 1.53

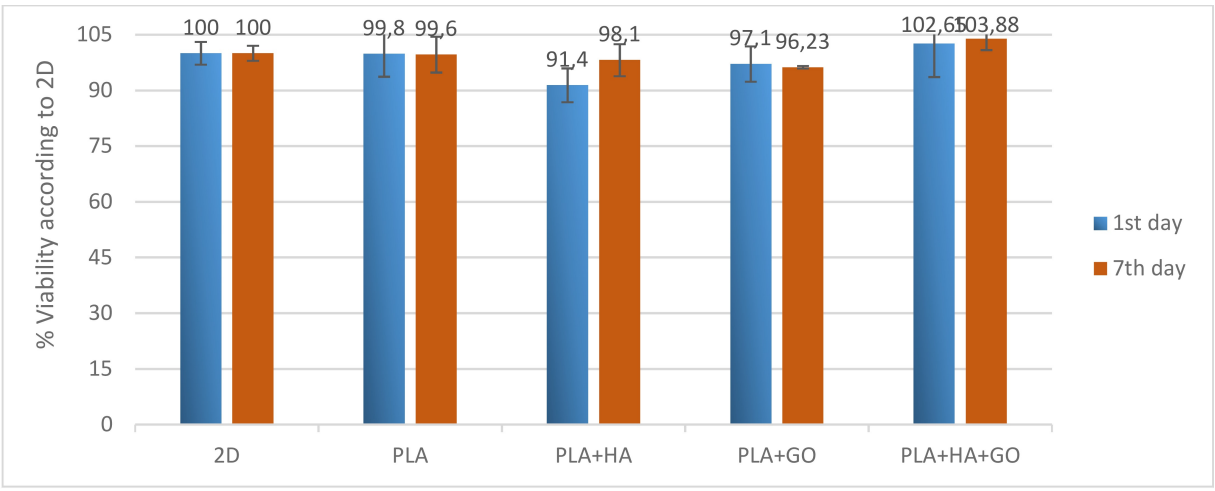

Figure 6. MTT test results of HFF-1 fibroblast cells cultured with scaffolds produced by electrospinning.

scaffold on the 1st day and 7th day after seeding was determined using the MTT assay. Figure 6 is showed cell viability of HFF-1 fibroblasts on fabricated scaffolds. When the PLA/HA/GO scaffold was compared to the pure PLA scaffold, the PLA/HA/GO scaffold exhibited increased cell viability on the 1st day and 7th day. The highest cell viability was 103.88% of the PLA/HA/GO scaffold on the 7th day. With the addition of HA and GO to PLA; PLA/HA/GO scaffolds have been observed to affect cell proliferation by providing a higher surface-to-volume ratio than pure PLA scaffolds. Looking at the results, the structure showing the highest biocompatibility is the PLA/HA/GO composite scaffold. Graphene oxide, which is formed by the oxidation of graphene, becomes a hydrophilic material thanks to its functionalized groups. The preservation of biocompatibility for the PLA/HA/GO scaffold is attributed to the excellent intrinsic biocompatibility and the hydrophilic nature of GO.[51] This is the result of the positive effect of the hydrophilic structure from GO on cell adhesion. Scaffold properties play an active regulatory role in controlling cell attachment.[52] According to all this information, the increase of HFF-1 cells in the porous scaffolds formed by electrospinning shows us that there is an interaction between the cell and the surface area of the scaffold that is suitable for cell behavior. As seen in Figure 6, cytotoxicity and cell adhesion experiments demonstrated the biocompatibility of PLA/HA/GO scaffolds. With all this information, the increase of HFF-1 cells in PLA/HA/GO porous scaffold formed by electrospinning shows that there is an interaction between cell and scaffold and the surface area of the scaffold is suitable for cell behavior. Thus, it is expected that the PLA/HA/GO scaffold can present the attachment, migration, and proliferation of cells in specific directions, and the presence of these features to increase cell proliferation and differentiation.

Cell Adhesion and Morphology

The morphology of cultured HFF-1 cells on the PLA/HA/GO scaffold was examined under SEM. When cell adhesion to the samples was examined (Figure 7), it was found that nano-

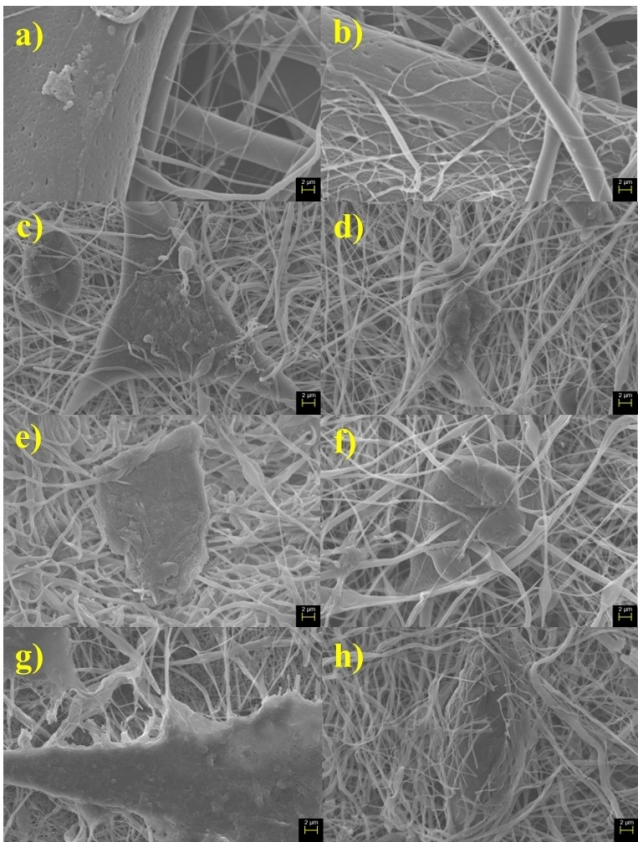

Figure 7. SEM images of HFF-1 cells grown on scaffolds produced by electrospinning; PLA scaffold on the 1st day (a) and 7th day (b) PLA/HA scaffold on the 1st day (c) and 7th day (d) PLA/GO scaffold on the 1st day (e) and 7th day (f) PLA/HA/GO scaffold on the 1st day (g) and 7th day (h).

structured scaffolds offered a good microenvironment for cells and supported cell attachment. In Figure 7, after HFF-1 fibroblast cells were seeded and incubated directly on their nanostructured scaffolds, it was seen that the surfaces of the scaffolds were covered with cells and ECM secreted by the cells. In Figure 7, it was seen that these cells spread to all scaffold surfaces on the 1st day, while it was observed that they penetrated into all the scaffold nets on the 7th day. It was also supported by SEM images that HFF-1 cells attached to all scaffolds and exhibited specific spindle-like morphologies. It was observed that cells grown on PLA/HA/GO scaffold were more prominent and interacted with the fiber structure than those grown on pure PLA scaffold. This indicates that either HA or GO mimics tissue and positively affects cell attachment and cell viability. Cells grew on the pure PLA scaffold but did not adhere to the scaffold. This is explained by the fact that PLA is a hydrophobic polymer. With the addition of GO, the penetration of cells into the scaffold was increased, owing to the increased hydrophilic properties in the scaffold. On the other hand, the penetration of cells into the scaffold by adding HA to the scaffold is due to the fact that HA is a bioactive material.[39] In addition, the roughness of the PLA/HA/GO scaffold and the increase in the surface area prepared the environment for the condensation of cells.[48] Cells grew on scaffolds and showed a distinct three-dimensional morphology with partial cell-cell interactions. According to SEM images, the strong adhesion and proliferation of cells on the scaffold supported the biocompatibility of PLA/HA/GO scaffold.

Cells grew on scaffolds and showed a distinct three-dimensional morphology with partial cell-cell interactions. DAPI dye is widely used in fluorescent microscope studies. The fluorescence images (Figure 8) that the previously dye-stained scaffolds with DAPI exhibited similar results obtained in the MTT assay. Because DAPI passes through the undeformed cell membrane and stains the nucleus, it can be used to stain both viable cells and fixed cells.[53] Because of this, it can be seen from Figure 8 that between the 1st and 7th days the number of cells on the pure PLA and PLA/HA/GO scaffolds increased notably. On the other hand, more increase in HFF-1 fibroblast cell density was observed in PLA scaffold containing HA and GO compared to pure PLA scaffold. This indicates that either HA or GO positively affects cell viability so that both are biocompatible. Accordingly, it is thought that the addition of HA which has a similar structure to bone mineral and GO which is an imitation of the natural structure, increases the cell adhesion on the scaffold and that these nanoparticle structures help cell aggregation.

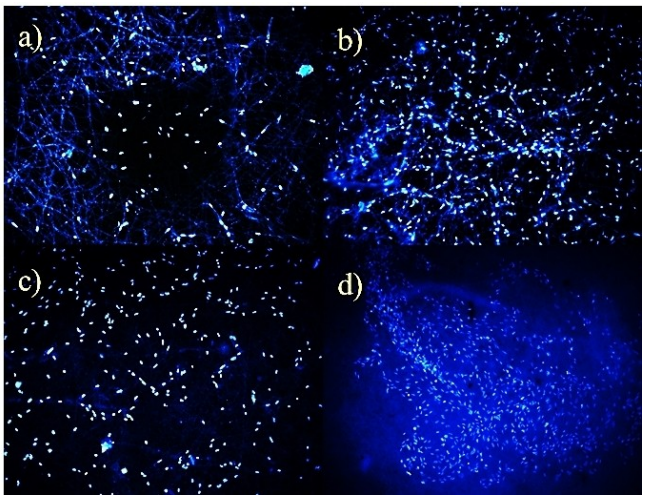

Figure 8. Fluorescent microscope images of HFF-1 cells grown on nanofiber scaffolds; PLA on the 1st day (a) and 7th day (b), PLA/HA/GO on the 1st day (c) and 7th day (d).

Conclusion

In this study, polymeric PLA nanofiber scaffold containing HA and GO nanoparticles that increase biocompatibility and bioactivity were fabricated using the electrospinning technique for tissue engineering applications. Powdered HA and GO were evenly distributed in the PLA matrix, and the resulting nanocomposite material retained the fibrous structure. The morphological, chemical, mechanical, and cytotoxic properties of the produced PLA, PLA/HA, PLA/GO and PLA/HA/GO nanofiber-structured bone scaffolds were examined in detail and the results were evaluated. According to SEM results, pure PLA nanofibers showed a beadless and smooth fiber structure, beaded structure was observed in PLA nanofibers containing HA and GO. In FTIR analysis, only the characteristic bands of PLA, which is the polymer were observed intensely. Tensile test results show that fiber samples have strength and elongation values in the appropriate range for tissue engineering applications. In vitro studies show that the scaffolds did not exhibit cytotoxicity, and HA and GO nanoparticles incorporated into the fiber structure supported cell viability and cell proliferation. Therefore, PLA/HA/GO nanofibers exhibited better biocompatibility compared to pure PLA nanofibers. It is thought that the biocompatible PLA/HA/GO nanofiber scaffold with effective potential for cell proliferation is suitable for tissue engineering applications. The combined advantages of PLA/HA/GO nanofiber composite scaffold, including porous fibrous 3D structure, biocompatibility, and mechanical properties from HA and GO, are believed to be promising material for tissue engineering applications.

Experimental PartMaterials

Polylactic acid (PLA 4060D) (Nature Works LLC.) was used in granule form. Trichloromethane ($CHCl_3$, Merck) was used to dissolve PLA as a solvent. N, N dimethylformamide (DMF, Merck) and dichloromethane (DCM, Merck) were used as a solvent to solve GO and HA. The solvents were used without further purification.

Preparing of Solutions

Firstly, GO and HA were obtained to produce PLA/HA/GO scaffold. Graphene oxide synthesis was carried out by the modified Hummers method.[41] Hydroxyapatite synthesis was carried out by wet precipitation.[42] 0.4 g of HA powders and 0.2 g of GO powders were dispersed by ultrasonication in 5 mL of DMF/DCM. The

solvent ratios of DMF and DCM were used as 2:3 *v*/v for GO and HA nanoparticles. After that, PLA particles were dissolved in $CHCl_3$ with the aid of stirring. In this precursor suspension, the percentage composition of PLA was 8 wt %. Then, HA and GO were dispersed in the PLA solution by ultrasonication. The final solution was stirred for 40 min (Schema 1).

Fabrication of nanofibers via electrospinning

Electrospinning process studies were carried out at different voltages and flow rates. The voltages were changed from 12 to 15 kV, while the flow rates varied from 0.5 to 0.7 mL/h to produce polymeric nanofibers. All the nanofibers were collected on grease-proof paper separately, and needle tip to collector distance was maintained as 15 cm. The size of the stainless-steel needle was 23-gauge. After the arranging of parameters, PLA, PLA/HA, PLA/GO, and PLA/HA/GO solutions were used to form nanofibers by electrospinning (Fytronix ESP 9000) machine.

Characterization of Electrospun Nanofibers

Crystal Structure Analysis of Nanoparticles

Crystal structure of GO and HA nanoparticles was characterized by X-ray powder diffraction (XRD) (X-ray diffraction analysis; X' Pert PRO PANalytical equipment) which has Cu Kα (λ = 1.54060 Å, 45 kV ve 40 mA) radiations with scanning speed of 3° 49 to 20° at 1°/min.

Chemical Structure Analysis

Chemical characterization of all nanofibers was investigated using Fourier Transform Infrared (FTIR) spectroscopy (JASCO 4700, USA) in the range of 4000–400 cm^{-1}. Samples turned into small clusters to take data.

Morphological Observation of the Nanofibers

The morphologies of the nanofibers (PLA, PLA/HA, PLA/GO, PLA/HA/GO) produced by the electrospinning method were observed by Scanning Electron Microscope (SEM, MA-EVO10, ZEISS, San Diego, CA, USA) at an accelerating voltage of 10 kV. Samples were cut into suitable sizes for observation before imaging.

Mechanical Testing

Mechanical tests were carried out using a tensile testing machine to measure the breaking strength and elongation at the break of nanofiber samples. Tensile tests were performed three times to determine the mechanical properties of the nanofiber samples. Before the tensile strength tests, two rectangular specimens which are 5 cm in length and 1 cm in width of each sample were cut. The thickness of each test specimen was measured using a high-accuracy digital micrometer (Mitutoyo, USA). The tensile strength and strain of all nanofibers were performed using a tensile tester (SHIMADZU, EZ-LX, China) by means of running special software. All samples were subjected to test at the speed of 5 mm/min until the breaking point. The measurements were carried out at room temperature.

Cell Culture Studies

Cell viability/MTT Assay

5×10^3 Fibroblast cells (HFF-1) were seeded onto the scaffolds in the 96 well plates like on standard cell seeding procedure after overnight ultraviolet (UV) light sterilization. At the same time, monolayer cell cultures were incubated with the same number of cells in 150 µl as a control. The cell-scaffold construct and monolayer cultures were incubated at 37 °C, 5 % CO_2 for 1, 3, and 7 days in a humidified incubator (NuAire). The toxic effect of scaffolds was checked on days 1, 3, and 7. To investigate cytotoxicity at a given time point, MTT (3-(4, 5-dimethylthiazolyl-2)-2, 5-diphenyltetrazolium bromide) (Glentham Life Sciences) cytotoxicity assay method was used according to manufacturer's protocol. The absorbance value of the cytotoxicity test was measured at 570 nm wavelength (690 nm as Ref. value) in ELISA reader (Enspire, Perkin Elmer). The assay was studied 3 times and the average of the results was considered as the final result.

Cell Adhesion and Morphology

Morphological analyzes of scaffolds were characterized using scanning electron microscopy (SEM, EVO MA-10). After 1,3 and 7 days of incubation, samples were fixed with 2.5 % glutaraldehyde (Sigma, St. Louis, MO, USA) for 2 h and then dehydrated through serial dilutions of ethanol (30 %, 50 %, 70 %, 90 %, and 99 %). Dried samples which were analyzed using SEM were sputter-coated with

Scheme 1. Production scheme of PLA/HA/GO nanofibers.

gold (SC 7620 model, Quorum Technologies, Sacramento, CA, USA) for 90 s and observed by SEM with an accelerating voltage of 10 kV.

Fluorescence Microscopy Analyses

The cells (5x10^3 cells) were incubated on each type of scaffold in 96 well plates with a standard cell seeding procedure. After 1, 3, and 7 days, the growth medium was discarded, and scaffolds were washed with 100 µl pre-warmed PBS three times. Following, the cells were initially fixed with 4% formaldehyde (Sigma) at room temperature for 15 min, washed and incubated with 0,1% Triton X-100 (Merck) to increase permeability for 10 minutes. Further 1/5000 DAPI (Invitrogen) was added to each sample and kept for 5 min at room temperature to stain the nucleus of the cells. Afterwards, DAPI solution was discarded, the scaffold was placed between the slide and coverslip and results were observed and captured under Florescence inverted microscope (Leica).

Conflict of Interest

The manuscript was written through the contributions of all authors. All authors have given approval to the final version of the manuscript. The authors declare no conflict of interest.

Data Availability Statement

The data that support the findings of this study are available from the corresponding author upon reasonable request.

Keywords: Bone Tissue Engineering · Graphene Oxide · Hydroxyapatite (HA) · Polylactic acid (PLA) · Scaffold

[1] A. Cheng, Z. Schwartz, A. Kahn, X. Li, Z. Shao, M. Sun, H. Chen, *Tissue Eng., Part B* **2019**, *25*, 14–29.
[2] S. H. Kelly, L. S. Shores, N. L. Votaw, J. H. Collier, *Adv. Drug Delivery Rev.* **2017**, *114*, 3–18.
[3] A. Eltom, G. Zhong, A. Muhammad, *Adv. Mater. Sci. Eng.* **2019**, 1–13.
[4] S. Bose, S. Tarafder, A. Bandyopadhyay, *Ann. Biomed. Eng.* **2016**, *45*, 261–272.
[5] B. P. Chan, K. W. Leong, *Eur. Spine J.* **2008**, *17(4)*, 467–479.
[6] D. Howard, L. D. Buttery, K. M. Shakesheff, S. J. Roberts, *J. Anat.* **2008**, *213(1)*, 66–72.
[7] S. Giwa, J. K. Lewis, L. Alvarez, R. Langer, A. E. Roth, G. M. Church, M. Toner, *Nat. Biotechnol.* **2017**, *35(6)*, 530–542.
[8] M. S. B. Kashte, PhD thesis, D. Y. Patil Education Society (India), **2019**.
[9] F. J. O'Brien, *Mater. Today* **2011**,*14(3)*, 88–95.
[10] L. Roseti, V. Parisi, M. Petretta, C. Cavallo, G. Desando, I. Bartolotti, B. Grigolo, *Mater. Sci. Eng. C* **2017**, *78*, 1246–1262.
[11] F. Shang, Y. Yu, S. Liu, L. Ming, Y. Zhang, Z. Zhou, Y. Jin, *Bioact. Mater.* **2021**, *6*, 666–683.
[12] H. Qu, H. Fu, Z. Han, Y. Sun, *RSC Adv.* **2019**, *9*, 26252–26262.
[13] F. M. Chen, X. Liu, *Prog. Polym. Sci.* **2016**, *53*, 86–168.
[14] B. Dhandayuthapani, Y. Yoshida, T. Maekawa, D. S. Kumar, *Int. J. Polym. Sci.* **2011**, *9(8)*, 679–697.
[15] N. Almouemen, H. M. Kelly, C. O'Leary, *Comput. Struct. Biotechnol. J.* **2019**, *17*, 591–598.
[16] E. Cosgriff-Hernandez, A. G. Mikos, *Pharm. Res.* **2008**, *25(10)*, 2345–2347.
[17] F. A. Sheikh, H. W. Ju, B. M. Moon, O. J. Lee, J. H. Kim, H. J. Park, C. H. Park, *J. Tissue Eng. Regener. Med.* **2016**, *10(3)*, 209–221.
[18] N. C. Hashim, D. Frankel, D. Nordin, *Ceram.-Silik.* **2019**, *63*, 426–448.
[19] B. Gürbüz, S. Ayan, M. Bozlar, C. B. Üstündağ, *Emergent Mater.* **2020**, *3*, 479–502.
[20] P. Chocholata, V. Kulda, V. Babuska, *Materials* **2019**, *12*, 568.
[21] M. Ansari, *Prog. Biomater.* **2019**, *8*, 223–237.
[22] M. Rahmati, D. K. Mills, A. M. Urbanska, M. Saeb, J. R. Venugopal, S. Ramakrishna, M. Mozafari, *Prog. Mater. Sci.* **2021**, *117*, 100721.
[23] M. S. Islam, B. C. Ang, A. Andriyana, A. M. Afifi, *SN Appl. Sci.* **2019**, *1(10)*, 1–16.
[24] M. N. Collins, G. Ren, K. Young, S. Pina, R. L. Reis, J. M. Oliveira, *Adv. Funct. Mater.* **2021**, *31*, 2010609.
[25] J. M. Ameer, A. K. Pr, N. Kasoju, *J. Funct. Biomater.* **2019**, *10*, 30.
[26] Y. Zhang, X. Liu, L. Zeng, J. Zhang, J. Zuo, X. Chen, *Adv. Funct. Mater.* **2019**, *29*, 1903279.
[27] L. Mckeen, The effect of sterilization on plastics and elastomers, DuPont, Wilmington, **2018**, p.319.
[28] T. Kim, C. W. See, X. Li, D. Zhu, *Eng. Regener.* **2020**, *1*, 6–18.
[29] P. Feng, J. Jia, S. Peng, Y. Shuai, H. Pan, X. Bai, C. Shuai, *Biomaterials* **2022**, *26(1)*, 1–15.
[30] C. Shuai, W. Yang, P. Feng, S. Peng, H. Pan, *Bioact. Mater.* **2021**, *6(2)*, 490–502.
[31] J. A. Wilson, D. Luong, A. P. Kleinfehn, S. Sallam, C. Wesdemiotis, M. L. Becker, *J. Am. Chem. Soc.* **2018**, *140(1)*, 277–284.
[32] J. L. Guo, Y. S. Kim, V. Y. Xie, B. T. Smith, E. Watson, J. Lam, A. G. Mikos, *Sci. Adv. Sci. Adv.* **2019**, *5(6)*, 1–12.
[33] G. Turnbull, J. Clarke, F. Picard, P. Riches, L. Jia, F. Han, W. Shu, *Bioact. Mater.* **2018**, *3(3)*, 278–314.
[34] C. L. Ko, W. C. Chen, J. C. Chen, Y. H. Wang, C. J. Shih, Y. C. Tyan, J. C. Wang, *Mater. Sci. Eng. C* **2013**, *33(6)*, 3537–3544.
[35] D. G. Papageorgiou, I. A. Kinloch, R. J. Young, *Prog. Mater. Sci.* **2017**, *90*, 75–127.
[36] C. Shuai, W. Guo, P. Wu, W. Yang, S. Hu, Y. Xia, P. Feng, *Chem. Eng. J.* **2018**, *347*, 322–333.
[37] H. Zhao, R. Ding, X. Zhao, Y. Li, L. Qu, H. Pei, W. Zhang, *Drug Discovery Today* **2017**, *22(9)*, 1302–1317.
[38] R. G. Bai, K. Muthoosamy, S. Manickam, A. Hilal-alnaqbi, *Int. J. Nanomed.* **2019**, *14*, 5753.
[39] C. Chen, X. Sun, W. Pan, Y. Hou, R. Liu, X. Jiang, L. Zhang, *ACS Sustainable Chem. Eng.* **2018**, *6*, 3862–3869.
[40] M. Gong, Q. Zhao, L. Dai, Y. Li, T. Jiang, *J. Asian Ceram. Soc.* **2017**, *5(2)*, 160–168.
[41] A. Jiříčková, O. Jankovský, Z. Sofer, D. Sedmidubský, *Materials* **2022**, *15(3)*, 920.
[42] A. Anwar, Q. Kanwal, S. Akbar, A. Munawar, A. Durrani, M. H. Farooq, *Nanotechnol. Rev.* **2017**, *6(2)*, 149–157.
[43] X. Li, Y. Su, S. Liu, L. Tan, X. Mo, S. Ramakrishna, *Colloids Surf. B* **2010**, *75(2)*, 418–424.
[44] C. Shuai, B. Peng, P. Feng, L. Yu, R. Lai, A. Min, *J. Adv. Res.* **2022**, *35*, 13–24.
[45] V. Loryuenyong, K. Totepvimarn, P. Eimburanapravat, W. Boonchompoo, A. Buasri, *Adv. Mater. Sci. Eng.* **2013**, *2013*, 1–5.
[46] C. Zhang, L. Wang, T. Zhai, X. Wang, Y. Dan, L. Turng, *J. Mech. Behav. Biomed. Mater.* **2015**, *53*, 403–413.
[47] A. Haleem, M. Javaid, R. H. Khan, R. Suman, *J. Clin. Orthop. Trauma* **2020**, *11*, S118–S124.
[48] N. T. Hiep, B. T. Lee, *J. Mater. Sci. Mater. Med.* **2010**, *21(6)*, 1969–1978.
[49] S. Mohamadi , *Infrared Spectrosc.: Mater. Sci., Eng. Technol.* **2013**, *1*, 213–232.
[50] M. A. M. Hussein, S. Ulag, A. S. A. Dena, A. Sahin, M. Grinholc, O. Gunduz, M. Megahed, *Int. J. Nanomed.* **2021**, *16*, 5133.
[51] H. Ma, W. Su, Z. Tai, D. Sun, X. Yan, B. Liu, Q. Xue, *Chin. Sci. Bull.* **2012**, *57(23)*, 3051–3058.
[52] L. Roseti, V. Parisi, M. Petretta, C. Cavallo, G. Desando, I. Bartolotti, B. Grigolo, *Mater. Sci. Eng. C* **2017**, *78*, 1246–1262.
[53] B. I. Tarnowski, F. G. Spinale, J. H. Nicholson, *Biotech. Histochem.* **1991**, *66(6)*, 296–302.

Submitted: February 21, 2022
Accepted: July 21, 2022